

A COMPUTATIONAL TOOL FOR THE REDUCTION OF NONLINEAR ODE SYSTEMS POSSESSING MULTIPLE SCALES

ROBERT CLEWLEY^{†‡}, HORACIO G. ROTSTEIN[†], AND NANCY KOPELL[†]

Abstract. Near an orbit of interest in a dynamical system, it is typical to ask which variables dominate its structure at what times. What are its principal local degrees of freedom? What local bifurcation structure is most appropriate? We introduce a combined numerical and analytical technique that aids the identification of structure in a class of systems of nonlinear ordinary differential equations (ODEs) that are commonly applied in dynamical models of physical processes. This ‘dominant scale’ technique prioritizes consideration of the influence that distinguished ‘inputs’ to an ODE have on its dynamics. On this basis a sequence of reduced models is derived, where each model is valid for a duration that is determined self-consistently as the system’s state variables evolve. The characteristic time scales of all sufficiently dominant variables are also taken into account, to reduce the model further. The result is a hybrid dynamical system of reduced differential-algebraic models that are switched at discrete event times.

The technique does not rely on explicit small parameters in the ODEs, and automatically detects changing scale separation both in time and in ‘dominance strength’ (a quantity we derive to measure an input’s influence). Reduced regimes describing the full system have quantified domains of validity in time, and with respect to variation in state variables. This enables the qualitative analysis of the system near known orbits (e.g. to study bifurcations) without sole reliance on numerical shooting methods.

These methods have been incorporated into a new software tool named DSSRT, which we demonstrate on a limit cycle of a synaptically driven Hodgkin–Huxley neuron model.

Key words. multiple scale methods, computational methods, bifurcation analysis, methods for differential-algebraic equations, analytic approximation of solutions, biophysical neural networks

AMS subject classifications. 33F05, 34E13, 37M20, 65L80, 74H10, 92-08, 92C20, 93B35

1. Introduction. Systems of ordinary differential equations (ODEs) arise commonly as models in the natural sciences. Many of these models involve nonlinear dynamics and exhibit complex behavior [26, 52]. To understand this behavior, it is useful to have tools that allow us to focus on salient features of the equations, and to dissect the qualitative structure of their dynamics.

There is an assumption of one or more explicit small parameters in many popular models that exhibit multiple scales, for instance the van der Pol [64], FitzHugh–Nagumo [18], Morris–LeCar [51] and Wilson–Cowan [71] oscillators, and other weakly-coupled oscillators [32, 41, 45, 49]. Typically these systems are amenable to a standard use of geometrical singular perturbation theory [14, 34] and invariant manifold theory [70]. The systems are first understood at ‘fast’ and ‘slow’ singular limits as the small parameter vanishes. Subsequently, technical results are invoked that prove qualitatively similar orbits lie close to the singular orbits when these sub-systems are matched [50] and the small parameter is re-introduced [17].

We investigate a more general case for initial-value problems in which we do not assume the presence of explicit small parameters. Instead, we assume that state-dependent coupling introduces ‘emerging’ scales—not just in the time domain, but also in terms of the *influence* of interactions between variables (which we define formally). We take the Hodgkin–Huxley (HH) model of nerve action potential generation [31, 37] as our principal example. In this system, we find there are times when there are *more* than two time or influence scales present (sometimes with a lack of strong separation), which may even swap their orders of magnitude during a typical oscillation [61]. The pulsatile nature of state-dependent synaptic coupling between neurons may create other emergent multiple scales in the dynamics of a biophysical neural network. Nonetheless, our approach applies to systems with explicit small parameters, and we briefly discuss our ideas in the context of the van der Pol system.

It is important to distinguish the type of reductions we consider here from those that are aimed at deriving simpler models from more sophisticated ones. There is a large body of literature focusing on the latter, especially in the context of neural systems [2, 18, 38, 39, 46, 48, 71]. Here,

[†]Center for BioDynamics and Department of Mathematics, Boston University, Boston, MA 02215, U.S.A.

[‡]Corresponding author: rhc28@cornell.edu

we assume that an appropriate model system has already been decided (typically a detailed, physiological model). Our approach is to ask what structure that model system possesses that gives rise to its dynamics of interest, and so reduce its *analysis* to that of a sequence of local bifurcation scenarios. That sequence tells a concise story of the most important interactions between variables near orbits of interest in the full system.

In this preliminary study we are concerned mainly with developing the notation and ideas behind the dominant scale method, and its instantiation in the software tool DSSRT (the *Dominant Scale System Reduction Tool*)¹. Currently, this software is designed for use with Mathworks' MATLAB. Using DSSRT we demonstrate the dominant scale method's application to a HH-type model of a single compartment neuron being driven to spike rhythmically by slow, periodic synaptic inhibition from an external source. This system serves as the basis for many types of detailed physiological models of excitable membranes, and provides us with an example of a limit cycle in a 5-dimensional, stiff, non-autonomous system, whose structure is nevertheless easy to intuit. We include the external input in anticipation of a future presentation of the method being applied to more general networks.

Previously, the HH system has been a subject of conventional asymptotic analysis (e.g. [38, 61]). The results of these studies aid the validation of our methods. Of course, our intention is to apply our methods to higher-dimensional systems, where intuition is less readily available and calculations are more difficult to perform by hand. Our analytic approach to a seven-dimensional biophysical model of an entorhinal cortex spiny stellate cell [57] uses similar principles of self-consistent partitioning of orbits into asymptotically-valid reduced (two-dimensional) regimes. This reduction allows for the study of some complex cell behavior such as the existence of sub-threshold oscillations and their coexistence with spiking [11]. Applying DSSRT to the stellate cell equations we find that the reduced regimes are consistent with those found in [57].

1.1. Overview of the paper. We begin by developing the concepts of events, epochs, and dominance for general ODE systems in §§2.2–2.6. In §2.7 we use these concepts to determine a sequence of local models in a neighborhood of a known orbit of a system. The concept of a variable's characteristic time scale is developed in §2.8, and illustrated for a van der Pol oscillator. In §2.10 such time scale information assists in the further reduction of epoch models into 'regimes'. The validation of the regime models is discussed in §2.11.

In §3.1 we introduce a Hodgkin–Huxley-type ODE system used throughout the rest of the paper to exemplify the application of the dominant scale techniques. In the rest of §3 we adapt the notation of the Hodgkin–Huxley equations so that we can apply the new concepts, and demonstrate in §4 the insight gained by applying our methods. In §4.4 we describe the use of the reduced regimes in studying the underlying structure of orbits as bifurcation scenarios. Application to a broader class of models, and other work in progress, is discussed in §5.

2. The dominant scale method.

2.1. Overview. This section introduces the terminology and notation needed to formally define the dominant scale method for general systems of ODEs, such that it is amenable to automation in a computer program such as DSSRT. New terms will be in **bold**. Although we are introducing many new definitions, we hope that the reader will come to appreciate the relative simplicity of the method by following the in-depth example in the later sections and by using this section as a reference guide.

In brief, the method consists of the following five steps, to be explained in more detail later:

(1) For an N -dimensional ODE system we compute an orbit of interest, denoted $\tilde{\mathbf{X}}(t)$. This might be an approximation to a stable periodic orbit, for instance. This will be referred to as a **reference orbit**. Its components will be labeled using a tilde: for instance, $\tilde{x}(t)$.

(2) Choose a single variable (which we denote y) on which to focus the analysis. Determine which variables influence y most dominantly along $\tilde{\mathbf{X}}(t)$, and at which times. This determines

¹The DSSRT software, with user and technical documentation, full source code, and examples, is available at <http://cam.cornell.edu/~rclewley/DSSRT.html>.

active and **inactive** variables. Changes in the status of active and inactive variables constitute **events**.

(3) Partition the time domain at the events. Produce a sequence of reduced **epoch** models of the system, relative to the variable in focus, by introducing (or eliminating) the dominant (non-dominant) variables (resp.), whenever they change at the events.

(4) Further simplify the reduced models by replacing variables that are ‘slow’ relative to y by appropriate constants, and those that are ‘fast’ relative to y by their asymptotic target values. (This step is akin to traditional fast-slow asymptotic reduction.)

(5) Minimize the number of distinct reduced models that constitute a piecewise model of the whole orbit by a heuristic consolidation of some models generated in step 3.

The result is a sequence of R **regime** models, focused on y near to $\tilde{\mathbf{X}}(t)$. Each model is a differential-algebraic equation (DAE), having dimension $\leq N$. Each DAE applies only in a neighborhood of one of the R temporal partitions of $\tilde{\mathbf{X}}(t)$, within which it can be studied using conventional qualitative techniques. We can explicitly determine the neighborhood within which the assumptions made in the regime reductions remain valid. Approximate orbits for the system may also be constructed using the regime model.

The focus on an individual variable reveals the fine structure of the dynamics most pertinent to it, by taking advantage of the known structure of the differential equation governing that variable. In principle, any variable of the system can be chosen as the focused variable, by repeating steps 2–5. Doing this for different variables creates alternative perspectives on the dynamics associated with the orbit $\tilde{\mathbf{X}}(t)$. Combining these perspectives in a simultaneous analysis of multiple variables is beyond the scope of our presentation, and creates complexities in the method which have not been fully resolved. We discuss this further in §5.4.

2.2. Assumed system structure. Consider a coupled ODE system given by

$$\frac{d\mathbf{X}}{dt} = \mathbf{F}(\mathbf{X}; \mathbf{s}, t), \quad (2.1)$$

where $\mathbf{X}(t) \in \mathbb{R}^N$, and $\mathbf{s} \in \mathbb{R}^S$ are external inputs (constants or time-varying signals). The aim of the method is to demonstrate when certain variables or inputs in Eq. (2.1) can be neglected during the computation of orbits of this system as an initial-value problem. We approach this by focusing on the structure of each differential equation making up Eq. (2.1). For any variable y of the system, let Γ_y denote the set of all variable names *and* external inputs that appear in the right hand side of the equation for y . Collectively these are called the **inputs** to the equation, and we define $n_{\text{tot}} \equiv |\Gamma_y| \leq N + S$ for that equation. Inputs that are variables of the system are called **dynamic inputs**. The external inputs are also called **passive inputs** because they are assumed to be fixed time-courses, independent from the ODE system given by Eq. (2.1). We can re-write the equation in y extracted from Eq. (2.1), having a right hand side (r.h.s.) given by a function F_y , in this general form:

$$\begin{aligned} \frac{dy}{dt} &= F_y(y, \{x\}_{x \in \Gamma_y}; t) \\ &\equiv \sum_{i=1}^{n_f} f_i(y, \{x\}_{x \in \Gamma_{1,i}}; t) + \sum_{i=1}^{n_g} g_i(\{x\}_{x \in \Gamma_{2,i}}; t), \end{aligned} \quad (2.2)$$

where $n_f > 0$, $n_g \geq 0$. Here we have separated the r.h.s. into a sum of **input terms**. We have also distinguished input terms that involve y (using the functions f_i) from those that do not (functions g_i). Each function depends on one or more of the other variables (or external inputs) in the system, according to **input sets** labeled $\Gamma_{1,i}$ for the f_i and $\Gamma_{2,i}$ for the g_i . In this notation we can allow *one* of the $\Gamma_{1,i}$ sets to be empty, if we wish to include a term depending solely on y . Such a term would be interpreted as governing the ‘internal’ or ‘intrinsic’ dynamics of y . We also define the sets $\Gamma_1 = \bigcup_i \Gamma_{1,i}$ and $\Gamma_2 = \bigcup_i \Gamma_{2,i}$, such that $\Gamma_1 \cup \Gamma_2 = \Gamma_y$. By assuming $n_f > 0$, the only restriction we are placing on the systems we consider is that each equation must depend explicitly on its own variable in its r.h.s.

We will always assume that the r.h.s. has been reduced to this form as far as possible. Most importantly for our method, this means that none of the functions f_i and g_i may be a sum of terms that could be separated into different input terms. Thus, input terms involving more than one input variable must consist of a product of functions of one variable only. The secondary criterion is to algebraically arrange the r.h.s. in a way that minimizes the size of the intersections of the input sets. For instance, consider a hypothetical r.h.s. $F_y(y, x_1, x_2) = x_1 y (\sin x_2 + ky)$, where k is a constant. By our rules, this cannot be treated as a single input term because $\sin x_2 + ky$ is a sum involving two different variables, such that the whole expression cannot be factored to be a product of functions of single variables. We have to expand the brackets to give $x_1 y \sin x_2 + kx_1 y^2$, at the small expense of letting x_1 appear in two input terms. If the r.h.s. had instead been $x_1 y (\sin x_2 + k)$ then we would not have to make any re-arrangement, because the bracketed term, although a sum, involves only one variable.

Clearly, in the general case, it is not always possible to avoid overlap between the input sets, regardless of how the r.h.s. is re-arranged. Dealing with these situations is beyond the scope of this paper. Here, we restrict our attention to systems in which this does not happen. This is not very restrictive given that the models to which our technique is perhaps most applicable are coupled networks drawn from systems biology and rigid body mechanics. These networks typically involve an input variable appearing in only a single input term per equation, so that there is never any overlap between the input sets.

2.3. The instantaneous asymptotic target. An important quantity in the dominant scale method is the **instantaneous asymptotic target** $y_\infty(t)$ of a *single* variable y . For any time t , the asymptotic target solves

$$F_y(y_\infty(t), \{\tilde{x}(t)\}_{x \in \Gamma_y}; t) = 0, \quad (2.3)$$

where the $\tilde{x}(t)$ are the entries of the vector $\tilde{\mathbf{X}}(t)$ corresponding to the inputs of Eq. (2.2). If F_y is smooth then at least one solution for $y_\infty(t)$ always exists. All solutions will be finite because we assume $n_f > 0$. A solution $y_\infty(t)$ is not necessarily a valid orbit of the system, but it always represents an instantaneous ‘organizing center’ for the dynamics of y in a neighborhood of $\tilde{\mathbf{X}}(t)$. Because we are mostly interested in systems with stable limit cycles we name y_∞ a ‘target’, but note that for any non-dissipative portions of a orbit the ‘target’ may be a repeller. However, the utility of $y_\infty(t)$ as a reference for the local organization of the vector field is the same in either case. Our definition of $y_\infty(t)$ coincides with that of the time-dependent y -nullcline for which the inputs $x \in \Gamma_y$ are restricted to the values $\tilde{x}(t)$. For dissipative systems in which $\tilde{\mathbf{X}}(t)$ is part of a normally hyperbolic invariant manifold [17, 34], y will always be attracted to (or repelled from) a nearby solution for $y_\infty(t)$. Parts of orbits that are not normally hyperbolic must be treated specially as boundary layers, and any expanding regions of the phase space would also require special treatment to ensure that validity conditions for their reduced models are always met. However, these aspects are beyond the scope of the present work.

2.4. Dominance strength. For some purposes it is reasonable to judge which input terms dominate the r.h.s. of an equation simply by comparing their magnitudes. This is probably the most straightforward approach to measuring ‘dominance’. However, we will see in §2.11 that our alternative approach offers several advantages in the local analysis of orbits.

The dominant scale method centers around the comparison of the sensitivities of $y_\infty(t)$ to the inputs $x \in \Gamma_y$. This requires that all the functions specifying the input terms are differentiable in the variables from their input sets. In the event that more than one input appears in a $\Gamma_{1,i}$ or $\Gamma_{2,i}$, then by assumption the inputs in that term are multiplied together in some way (§2.2). In this case we must select one to be the **primary** variable for analysis, while the remaining input variables in the input term are referred to as **auxiliary** variables. This assumes that the auxiliary variables can be selected to be those of ‘lesser importance’—in particular, that they can be interpreted as modulators of the primary variable. We need this distinction because here we only consider the input term’s sensitivity to variation in one variable. When multiple inputs to a single term cannot

be meaningfully distinguished as primary and auxiliary we require a more intricate treatment that is beyond the scope of this paper.

The sensitivities of y_∞ are referred to as **dominance strengths**. The dominance strength of an input involving the primary variable x to the r.h.s. F_y is denoted by Ψ_x . For ease of notation its association with y remains implied because no ambiguity will arise in its use here. It is defined as

$$\Psi_x(t) = \left| x(t) \frac{\partial y_\infty}{\partial x}(t) \right|. \quad (2.4)$$

The factor of x that multiplies the partial derivative acts to normalize it, on the assumption that $x = 0$ means ‘no input’ (a linear transformation of variables can always ensure this). The normalization is made because we prefer not to characterize a non-participatory input $x(t) \equiv 0$ as dominant over y if the partial derivative evaluated at $x = 0$ is large. Apart from the normalizing factor, the dominance strength resembles a sensitivity with respect to perturbations on an input rather than initial condition.

Depending on the nature of the system, the derivatives in the dominance strength calculations may have to be calculated numerically. Under some circumstances, such as those that arise for the class of neural model we introduce in §4, y_∞ and its derivatives may exist in closed form. The DSSRT program takes advantage of such a circumstance.

We note that if a term in F_y has no inputs, then it has no associated dominance strength, and is not subject to being eliminated in the reductions discussed here. For generality, we allowed one such term in F_y when making our assumptions about Eq. (2.2).

2.5. Active and inactive inputs. For each $x \in \Gamma_y$, DSSRT calculates $\Psi_x(t)$ along the known orbit $\tilde{\mathbf{X}}(t)$. At a sufficiently fine time resolution, DSSRT ranks the dominance strengths for each of these inputs by size for each sample time t ,

$$\Psi_{x_1} \geq \Psi_{x_2} \geq \dots \geq \Psi_{x_{n_{\text{tot}}}},$$

where the ordered list $\{x_i\}_{i=1\dots n_{\text{tot}}}$ is a permutation of Γ_y . We define the ranking in a ratio form, so that $\Psi_{x_i} = c_i \Psi_{x_1}$, where the coefficients $c_i \in (0, 1]$ define the **scale** of the i^{th} input relative to the strongest input x_1 . We do not necessarily have the convenience of an *explicit* small parameter in our system, so we introduce a free parameter $\varepsilon \in (0, 1)$ that defines a small scale of influence between variables (typically not close to 0). Inputs having a scale coefficient $c_i \geq \varepsilon$ are called **active inputs** at time t , and form the ordered set of actives, $\mathcal{A}_{y,\varepsilon}(t)$. $\mathcal{A}_{y,\varepsilon}(t)$ is a piecewise-constant function of the continuous time t . The remaining inputs are **inactive** at time t . By defining the set of actives *relative* to the largest $\Psi_x(t)$ value, the meaning of dominance—i.e. the ‘ $\mathcal{O}(1)$ scale of influence’—is continually renormalized along an orbit.

For input terms that involve more than one input variable, where one is primary and the others are auxiliary, our convention is to record only the primary variable in $\mathcal{A}_{y,\varepsilon}$ —the presence of the auxiliary variables is implicit. The parameter ε must be set appropriately by the user for the method to be most effective. For instance, increasing ε causes DSSRT to produce increasingly reduced models at the expense of accuracy. Thus, ε effectively defines an error tolerance in the method.

2.6. Events and epochs. With knowledge of the full system’s equations, we characterize the underlying structure of $\tilde{\mathbf{X}}(t)$ by recognizing a sequence of important events that shaped its evolution. We define an **event** relative to a variable y as occurring whenever there is a change in the set of actives $\mathcal{A}_{y,\varepsilon}(t)$. We partition $\tilde{\mathbf{X}}(t)$ according to the times of these events, and we define an **epoch** as the time interval between consecutive events. For a given ε , DSSRT detects $P \equiv P(\varepsilon)$ events along an orbit and partitions the orbit into $P - 1$ epochs, having time intervals $[t_p, t_{p+1})$ for $p = 1, \dots, P - 1$. This results in an **epoch sequence** of distinct $\mathcal{A}_{V,\varepsilon}$ sets, each associated with one of the epochs.

2.7. Local epoch models. We use the definition of dominance strength to determine approximate local models to study the system in a neighborhood of $\tilde{\mathbf{X}}(t)$, *independent* of the relative time scales of the variables. DSSRT therefore needs accurate knowledge of the time-courses of the variables making up $\tilde{\mathbf{X}}(t)$ (e.g. from a numerically integrated solution). Within the p^{th} epoch a suitable reduced model of the system, focused on a variable y , is given by

$$\frac{dy}{dt} = \hat{F}_y(y, \{x\}_{x \in \hat{\Gamma}_y(t)}; t), \quad (2.5)$$

$$\left\{ \frac{dx}{dt} = F_x(x, \{z\}_{z \in \Gamma_x(t)}; t) \right\}_{x \in \hat{\Gamma}_y(t)}. \quad (2.6)$$

These equations hold for $t \in [t_p, t_{p+1})$, and we have defined $\hat{\Gamma}_y(t) = \mathcal{A}_{y, \varepsilon}(t) \cap \Gamma_y$, and \hat{F}_y to be the function F_y without the input terms contributed by the inactive variables. (The equations for any auxiliary variables are implicitly included whenever a primary variable $x \in \hat{\Gamma}_y(t)$.) The size of the neighborhood within which a local model applies can be prescribed analytically and computed numerically (§2.11).

In order to make a local comparison of the reduced model's approximation of $\tilde{\mathbf{X}}(t)$, the initial conditions for the model should be set to coincide with the corresponding entries of $\tilde{\mathbf{X}}(t_p)$. To construct other orbits that are close enough to $\tilde{\mathbf{X}}(t)$ so that they undergo the same sequence of events, the epoch switching times $\{t_p\}$ and the initial conditions of the epoch models at those times have to be determined self-consistently by ongoing analysis of the evolving orbit. (Further details are given in §2.11 and §4.4).

2.8. Time scales of inputs. As part of reducing epoch models further in §2.10, and in computing some properties of these models, we will need to estimate the reaction of a variable to $\mathcal{O}(1)$ perturbations at different points along $\tilde{\mathbf{X}}(t)$. In general, we define an $\mathcal{O}(1)$ perturbation from $\tilde{\mathbf{X}}(t)$ to be one that does not cause a change either in the set of actives or in the asymptotic targets that apply at time t . Our automated method addresses the robustness of a system to such perturbations by computing and comparing the **instantaneous time scales** τ_y and τ_x . We define

$$\tau_y(t) = \frac{y_\infty(t) - \tilde{y}(t)}{\dot{y}(t)}, \quad (2.7)$$

where $\dot{\cdot} = d/dt$, and we evaluate $y_\infty(t)$ and $\dot{y}(t)$ along $\tilde{\mathbf{X}}(t)$. We define $\tau_x(t)$ similarly. Using the notation $\boldsymbol{\tau}(t) = (\tau_x(t), \tau_y(t))$, we define the **time scale sensitivity matrix**, denoted $\partial\boldsymbol{\tau}/\partial\tilde{\mathbf{X}}(t)$. Entries in this matrix will also be needed in our analysis. Sometimes these quantities are given in closed form if the equations explicitly contain terms of this type, or if the algebraic make-up of a right hand side allows one to be factored out. Both of these cases arise in the class of neural equations studied later. Note that only the *dynamic* inputs to the differential equation for y have an associated time scale, because the passive inputs are not governed by differential equations (§2.2). Intuitively, we can observe in Eq. (2.7) that $1/\tau_y$ is a normalized measure of the instantaneous rate of change of y , where we have normalized by the distance between y and its instantaneous asymptotic target. $1/\tau_y$ can be loosely interpreted as an ‘instantaneous eigenvalue’ of the linearized dynamics of Eq. (2.2) about $y_\infty(t)$, where we view $y_\infty(t)$ as an ‘instantaneous fixed point’ of Eq. (2.2).

Because we do not assume explicit small time scales, we must define another free parameter, $\gamma \in (0, 1)$. When $|\tau_x(t)/\tau_y(t)| < \gamma$, a dynamic input $x \in \Gamma_y$ is considered ‘fast’ relative to y in its response to $\mathcal{O}(1)$ perturbations. Conversely, when the ratio is greater than $1/\gamma$, x is considered ‘slow’ in its response. Therefore, relative to a variable y in focus, a dynamic input can have one of three time scale classifications at any point in time: $\mathcal{O}(1/\gamma)$ -slow inputs are denoted by the set $\mathcal{S}_{y, \gamma}(t)$; $\mathcal{O}(\gamma)$ -fast inputs are denoted by the set $\mathcal{F}_{y, \gamma}(t)$; and $\mathcal{O}(1)$ (‘normal’ time scale) inputs are defined by exclusion from the other sets, i.e. by $\Gamma_y \setminus (\mathcal{S}(t) \cup \mathcal{F}(t))$.

Our approach is easiest to illustrate in a familiar setting. Consider the van der Pol system [64]

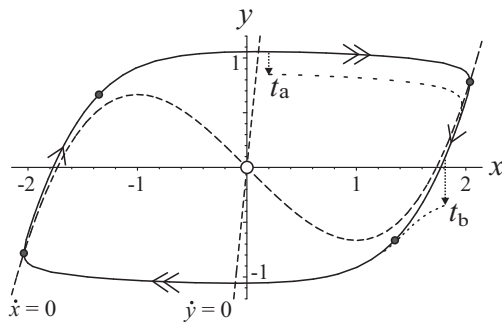


FIG. 2.1. The phase plane of a van der Pol oscillator. The stable limit cycle (solid line) is shown superimposed on its nullclines (dashed lines). An unstable fixed point is shown at the origin where the nullclines cross. Arrows show the direction of motion. Double arrows indicate portions of the orbit that are fast. Dotted lines indicate the effects of instantaneous perturbations in the y direction at times t_a and t_b . Solid circles mark the transitions from ‘slow’ to ‘fast’ regimes.

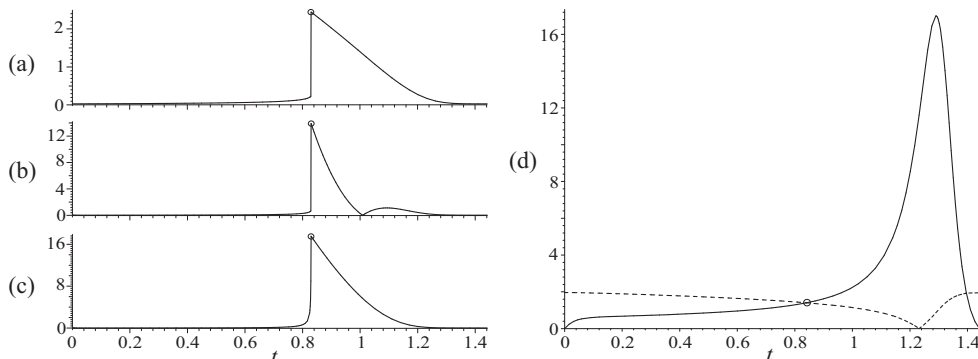


FIG. 2.2. (a) $|\tau_x|$, (b) $|\partial\tau_x/\partial x|$, and (c) $|\partial\tau_x/\partial y|$, plotted over $t \in [0, T/2]$. The circle at $t_{\text{crit}} \approx 0.840$ marks the departure from a stable branch of the slow manifold to a fast jump. The other stable branch of the slow manifold is reached at $t = T/2$. (d) $|dx/dt|$ (solid line) and $|dy/dt|$ (dashed line) are plotted over $t \in [0, T/2]$, with a marker at t_{crit} , where the velocities are equal.

expressed by the equations

$$\begin{aligned} \frac{dx}{dt} &= \mu \left(y + x - \frac{x^3}{3} \right), \\ \frac{dy}{dt} &= \nu y - x. \end{aligned} \quad (2.8)$$

We assume that the positive parameters μ and ν are chosen so that system has a stable limit cycle around the unstable fixed point at the origin. The limit cycle is denoted $\tilde{\mathbf{X}}(t) = (\tilde{x}(t), \tilde{y}(t))$, which also defines its components. The limit cycle and the nullclines are plotted in Fig. 2.1 for $\mu = 10$, $\nu = 0.1$. Here, x undergoes fast ‘jumps’ between two stable branches of the slow manifold that are close to the cubic x -nullcline. We assume that the system is evolving close to $\tilde{\mathbf{X}}(t)$, which, after a short transient, will be the case for all initial conditions chosen away from the origin.

The dominance strength quantities defined in §2.4 do not apply to the van der Pol system because each differential equation has only one input (the other variable of the system). In other words, y is *always* an active input to the equation for x , and vice versa. Also, the asymptotic target $x_\infty(t)$ is given by the appropriate branch of the cubic nullcline as $\tilde{\mathbf{X}}(t)$ evolves between the two stable branches of the slow manifold. As a result of these observations, $\mathcal{O}(1)$ perturbations for the van der Pol system are simply those that do not force orbits to switch between branches of the slow manifold. Geometric and asymptotic techniques can be applied to understand the robustness of the limit cycles as $1/\mu \rightarrow 0$ (known as the singular limit) [14, 22, 34], but we will now see how

the instantaneous time scale quantities defined in Eq. (2.7) can be used to study robustness away from this limit.

For $\mu = 10$ and $\nu = 0.1$, the period of the limit cycle is $T \approx 2.883$. We observe that $y_\infty = x/\nu = 10x$, and we take $x_\infty(t)$ to be the appropriate branch of the cubic nullcline, depending on the location of the orbit. We find that $\tau_y = -1/\nu = -10$, so that $y_\infty(t)$ is in fact a repeller. τ_x has a complicated (but explicit) form, which is plotted in Fig. 2.2(a). From this plot it is easy to calculate that $|\tau_x/\tau_y| \approx 0$ all along the limit cycle, although this ratio rises to nearly $1/4$ in the vicinity of certain ‘critical points’. The critical points are the positions in the cycle when the orbit moves from a slow to a fast manifold, or vice versa. They are marked by closed circles in Fig. 2.1. (As $1/\mu \rightarrow 0$ the critical points converge to the ‘knees’ of the cubic nullcline.) Away from the critical points we also find that the time scale sensitivity matrix entries for τ_y are identically zero, and $|\partial\tau_x/\partial x|$ and $|\partial\tau_x/\partial y|$ are shown in Fig. 2.2(b) and (c) to be almost zero. This indicates that $\mathcal{O}(1)$ perturbations in either variable hardly affect τ_x , and do not affect τ_y : in other words, that the separation of time scales is robust. The increased sensitivity of τ_x near the critical point at $t_{\text{crit}} \approx 0.840$ has decayed by $t = 1.2$, when the orbit is at approximately $(-0.21, 1.05)$. This position is only a small spatial distance from the critical point relative to the size of the fast jump. The sensitivity of the dynamics in small neighborhoods of the critical points is known to be important in understanding canard behavior [25, 44].

From measuring the time scale separation around the limit cycle it is reasonable to choose $\gamma = 1/4$, so that DSSRT determines x to be a ‘fast’ variable relative to y over the entire cycle (we re-iterate that we mean fast in its *response* to perturbations, not according to its velocity). Then, by focusing on the variable x , a reasonable model for its dynamics in this situation is to make the reduction $dy/dt = 0$, which is analogous to studying the ‘fast system’ in singular perturbation theory. Conversely, by focusing our method on the slow variable y , we can make the reduction $x(t) = x_\infty(t)$, which is analogous to studying the ‘slow system’. The sudden changes in τ_x and its sensitivities quantitatively indicate the shrinking of the neighborhoods around the limit cycle within which these reductions apply. These reduction steps are fully described in §2.10 for the general case.

Comparing the time scale quantities can help us avoid the costly computation and comparison of actual perturbed orbits. Near $\tilde{\mathbf{X}}(t)$ we can predict whether variables will remain essentially unchanged after a perturbation, or whether they will remain near to their perturbed values. A technique to do this is explained in §2.11, but here we take a brief look at the ideas involved using the van der Pol example. Consider two scenarios shown in Fig. 2.1, in which we perturb y at a time t_a or t_b along the limit cycle. The system undergoes a fast jump between stable branches of the slow manifold over the time interval $(t_{\text{crit}}, T/2)$. The fast manifold traversed during the jump is not normally hyperbolic, and locally the vector field is almost horizontal. Thus, a perturbation at time $t_a \in (t_{\text{crit}}, T/2)$ hardly alters the motion of x , which continues to relax quickly to a slightly perturbed position on the right-hand branch of the slow manifold. By the time the slow manifold is reached, y has only changed slightly from its perturbed value. The same outcome can be predicted by observing that the scale separation $|\tau_x(t_a)| \ll |\tau_y(t_a)|$ is very robust in a neighborhood of $\tilde{\mathbf{X}}(t_a)$. In fact, this observation predicts a qualitatively similar response of the system to $\mathcal{O}(1)$ perturbations throughout $(t_{\text{crit}}, T/2)$. In contrast, $|dx/dt| \gg |dy/dt|$ only for a small part of the jump (Fig. 2.2(d)), because the system is far from the singular limit. Therefore, it is more informative to compare the instantaneous time scales than the velocities in order to understand the effect of perturbations, and to characterize the separation of time scales far from the singular limit. At t_b , the macroscopic motion of the system is dominated by y ’s slow dynamics ($|dx/dt| < |dy/dt|$ along the slow manifold), provided it remains close to the limit cycle. However, the *reaction* of the system to a perturbation in y near the slow manifold is still controlled by the fast *response* of the x sub-system compared to y , i.e. because $|\tau_x| \ll |\tau_y|$. Again, the characteristic time scales allow us to effectively predict the outcome of perturbations. Similar arguments apply if we had instead perturbed x .

2.9. Potentially active inputs. Although a dynamic input may not be active at time t , it is possible that it would have been active if the input variables had taken different values (often,

values that are larger in magnitude). In such a case, these inputs are said to be **potentially active** at time t , and belong to the set $\mathcal{P}_{y,\varepsilon}(t)$. DSSRT determines when this is the case through a constrained maximization of the dominance strengths for the inputs. User-specified bounding intervals for the system's variables provide the constraints. Although gating variables for physiological models are typically designed to vary within the unit interval, *a priori* bounds are often unavailable. In the latter case it is sufficient to specify *effective* bounds. This can be done by conservatively estimating the extent of the variables' motion (in a volume containing $\tilde{\mathbf{X}}(t)$) over a range of 'typical' initial conditions, external inputs, and perturbations.

The presence of a potentially active input in the r.h.s. of Eq. (2.2) at a given time indicates a sensitivity of y 's dynamics to possible fluctuations in the corresponding input variable. Conversely, absence of an input from $\mathcal{P}_{y,\varepsilon}(t)$ means that the y dynamics are less than $\mathcal{O}(\varepsilon)$ -dominated by any variation in that input at time t . $\mathcal{P}_{y,\varepsilon}(t)$ provides information about the robustness of orbits in addition to what we discussed in the previous section. For instance, knowledge of $\mathcal{P}_{y,\varepsilon}(t)$ over one period of a stable oscillation could be used to determine the necessary timing and amplitude for effective modulation of the oscillation. In this case, $\mathcal{P}_{y,\varepsilon}(t)$ would serve a similar purpose to a 'phase response curve' [15, 72] or a 'spike-time response curve' [3]. During the construction of orbits via reduced models, DSSRT also tracks potentially active inputs as possible bifurcation parameters or as other sources of regime switching (see §2.11 and §2.12).

2.10. Reduced dynamical regimes. As we will see in the Hodgkin–Huxley example, the sequences of events that our method generates for ODE systems can be highly detailed. When compared to the results of standard matched asymptotic analysis of those equations by hand, the epoch sequences may appear to reflect not only intuitively crucial changes in the system, but also relatively inconsequential ones. As a result, DSSRT incorporates an algorithm that captures some of the intuition of matched asymptotic analysis for initial-value problems. It simplifies the sequence of P events by consolidating the minor changes to the system and only indicating the need to change a local model when certain crucial changes in the dynamics occur. The full details of the regime determination algorithm's implementation and use are too lengthy and technical to present here, so we limit ourselves to a summary of its major elements.

For periodic orbits, the first regime is started at an optimal point in the epoch sequence; otherwise it is started wherever $\tilde{\mathbf{X}}(t)$ begins. Epochs are added to the regime incrementally until the algorithm decides that circumstances have changed significantly enough that a new regime should be started. The set of variables accumulated from all the added epochs prescribes a regime model that is focused on y , in the same way as described by Eqs. (2.5)–(2.6) for the epoch models.

There are a variety of controls over the algorithm in DSSRT, but in its simplest form it dictates the following. Two epochs that differ only by passive variables are put in the same regime. A new regime is started whenever a fast variable $x \in \mathcal{F}_{y,\gamma}$ joins $\mathcal{A}_{y,\varepsilon}$. A new regime is also started when a fast variable leaves $\mathcal{A}_{y,\varepsilon}$, unless the resulting regime would have no dynamic variables remaining in its active set, and no quasi-static bifurcation variables left to track. Were a regime to be started in the latter situation, it would be trivial in its dynamics because its reduced equations would involve only passive input terms. Furthermore, in the absence of dynamic inputs or quasi-static bifurcation parameters the regime would be devoid of any achievable condition that could end its reign.

Time scale information was not used in the determination of events or epoch models. We will now give a flavor for how the algorithm uses this information to further reduce the dimension of a regime's local model. In certain circumstances, fast active variables $x \in \mathcal{F}_{y,\gamma}(t) \cap \mathcal{A}_{y,\varepsilon}(t)$ may be **adiabatically eliminated**, such that we set $x(t) = x_\infty(t)$ in the regime model. One condition that allows this is if $y \notin \mathcal{P}_{x,\varepsilon}(t)$. In this case, y can vary according to Eq. (2.5) in a neighborhood of $\tilde{y}(t)$, and x_∞ will change by no more than $\mathcal{O}(\varepsilon)$ over $\mathcal{O}(1)$ time durations. The adiabatic elimination can proceed provided the regime does not grow too long (i.e. to an $\mathcal{O}(1/\gamma)$ or $\mathcal{O}(1/\varepsilon)$ length, whichever is shorter). Conversely, if $y \in \mathcal{P}_{x,\varepsilon}(t)$, then y 's evolution may cause x_∞ to vary substantially from its known value (evaluated along $\tilde{x}(t)$), or τ_x may change such that $x \notin \mathcal{F}_{y,\gamma}$. One of the following cases will apply:

- $y \notin \mathcal{A}_{x,\varepsilon}(t)$. This means that there is a neighborhood around $\tilde{y}(t)$ within which x will

remain $\mathcal{O}(\varepsilon)$ -close to $\tilde{x}(t)$. Within this neighborhood, x_∞ can be reasonably estimated by its value evaluated along $\tilde{x}(t)$, provided the regime does not grow too long. Additionally, if $|\partial\tau_x/\partial y|$ is small along $\tilde{x}(t)$, then any changes induced in τ_x in the neighborhood around $\tilde{y}(t)$ will occur much more slowly than the attraction of x to its instantaneous asymptotic target, and we can proceed with the elimination. The neighborhood can be explicitly calculated.

- $y \in \mathcal{A}_{x,\varepsilon}(t)$. This means that $\mathcal{O}(1)$ changes in y will cause $\mathcal{O}(1)$ changes in x , and we do not have an easy way to estimate a neighborhood within which the adiabatic elimination will be accurate. Therefore, we do not proceed with the elimination.

Slow active variables in $\mathcal{S}_{y,\gamma}(t)$ that also have weak time scale sensitivity to y are replaced in the regime with an appropriate constant value, provided the regime does not become too long. The constant value is determined self-consistently from looking at neighboring regimes. Consistency checks similar to those needed for the adiabatic eliminations are required.

The result of this process is a number $R \leq P$ of consolidated events, defining $R - 1$ **reduced dynamical regimes**. The regimes tell a concise story of the most important interactions between variables evolving in a neighborhood of $\tilde{\mathbf{X}}(t)$, *from the perspective of a single variable*. Due to the consolidation of the events, the regimes are delimited by time intervals $[t_r, t_{r+1})$, where $r = 1, \dots, R-1$, and $\{t_r\} \subseteq \{t_p\}$. The checks required for determining the time-scale based reductions form part of the validity conditions discussed in the next section.

2.11. Regime validity conditions and robustness. As well as studying perturbation properties of $\tilde{\mathbf{X}}(t)$ relative to a variable y , we can use the regime models to construct new orbits close to $\tilde{\mathbf{X}}(t)$. Care must be taken to ensure that such orbits accurately represent true orbits of the full system (at least qualitatively) by the continual verification of various validity conditions. These conditions can be posed as tests for zero crossings in algebraic functions of the system's variables, their dominance strengths, their time scales, and so forth. These augment the differential equations for the regime to yield a set of differential-algebraic equations for the regime [62]. This also means that the collection of reduced models can be viewed as a hybrid dynamical system [65]. We consider an $(N + 1)$ -dimensional volume $\mathcal{D} \equiv \mathcal{D}(\varepsilon, \gamma) \subset \mathbb{R}^N \times \mathbb{R}$ around $\tilde{\mathbf{X}}(t)$, which is the largest volume within which the validity conditions for constructed orbits hold true. We refer to this volume as the local **domain of validity** (d.o.v.) for the reduced regimes. Self-consistency also requires that all orbits constructed during the r^{th} regime lie entirely within $\mathcal{D}|_{t \in [t_r, t_{r+1})}$. We can make use of our explicit knowledge of the equations and the values of ε and γ to calculate \mathcal{D} . This validation process is *asymptotically accurate*, i.e. it can prescribe the d.o.v. precisely only in the limit of vanishingly small ε and γ . Thus, ε and γ determine error tolerances for the accuracy of the computed d.o.v. Before describing DSSRT's method of estimating the d.o.v., we describe the three types of regime validity condition in detail.

(1) A regime becomes invalid if the sets of actives or the time scale classifications computed along constructed orbits (or as a result of perturbations from the reference orbit $\tilde{\mathbf{X}}(t)$) deviate substantially from those determined for $\tilde{\mathbf{X}}(t)$. Therefore, a deviation of this kind must not occur during the time evolution of the variables that are explicitly modeled in the regime.

(2) In the full ODE system given by Eq. (2.1), the motion of the variables explicitly modeled in a reduced dynamical regime may both affect and depend on the motion of the coupled variables that are not modeled. Thus, to have confidence in the accuracy of the regime model's dynamics, we must verify that the regime's assumptions are not invalidated by virtue of implied changes in the *un-modeled* variables of the system. We define a **shadowing error** to occur if the neglected feedback from the un-modeled dynamics causes enough error to accumulate in the construction of an orbit such that the regime's assumptions about $\mathcal{A}_{y,\varepsilon}$, $\mathcal{F}_{y,\gamma}$, and $\mathcal{S}_{y,\gamma}$ become invalidated. Shadowing errors are subtle and hard to detect because the reduced model may continue to produce plausible-looking orbits, whereas the full system starting from the same initial conditions could have significantly diverged. Of course, it is not generally desirable to compute the orbits of the full system in order to validate those constructed using a reduced model. An existing body of literature, concerning the error analysis of numerical solutions of ODEs, develops theories of shadowing more rigorously [29, 53]. We return to the practical implementation of conditions (1)

and (2) in DSSRT shortly.

(3) The local models of consecutive regimes involve different constituent variables (usually with some overlap). This forces us to address the validity of passing the projection of the full N -dimensional system between the low-dimensional models at discrete time events. Therefore, DSSRT must ensure that the correct ‘structural’ changes occur in the system as a constructed orbit progresses beyond the remit of the current regime, in comparison to the known changes along the reference orbit. If such a condition fails, then DSSRT will not know which regime to hand over control to. This is especially relevant to regime transitions in which the local model *gains* variables, since a previously inactive (i.e., not modeled) variable needs to have an appropriate initial condition after the transition. The regime determination algorithm attempts to determine which slowly changing or potentially active variables (in $\mathcal{P}_{y,\varepsilon}$) need to be tracked in order for DSSRT to accurately predict a transition into the next regime. These are known as the **quasi-static bifurcation parameters** for the regime. The magnitude of these variables must be tracked over the course of the preceding regime because they may be crucial in causing the local model to undergo a bifurcation (§2.12) or a change in time scale relationships. Such events signal that control of the dynamics should be passed to the next regime of the sequence generated for the reference orbit. A concrete example using this condition is given at the end of §4.4.

The remainder of this section is an overview of the most important factors used in the self-consistency checks implemented by DSSRT. To verify conditions (1) and (2) in practice, DSSRT requires estimates of the time scales and asymptotic targets of the variables in a neighborhood of the reference orbit. Together with their sensitivities to small variation in the un-modeled variables, these quantities can provide DSSRT with enough confidence that the positive feedback loops which cause the shadowing errors are unlikely. A simple example of testing these conditions was given in §2.8 for a van der Pol system. Also, tests relating to changes in the system’s time scale relationships were discussed in more detail at the end of the previous section. Currently, DSSRT does not fully implement these tests. Instead, DSSRT estimates the d.o.v. in the following *conservative* way.

Over a high-resolution set of sample times $\{t_s\}$ taken over the duration of the reference orbit, a variable y of the full system is perturbed from its values $\tilde{y}(t_s)$ to values we denote by $y^*(t_s)$. If the set of actives $\mathcal{A}_{y,\varepsilon}(t_s)$ and the time scale relationships given by $\mathcal{F}_{y,\gamma}(t_s)$ and $\mathcal{S}_{y,\gamma}(t_s)$ are not changed by a perturbation at t_s , then y^* is included in the restriction of the d.o.v. to the y -direction, denoted $\mathcal{D}|_y$, at the sample time t_s . DSSRT performs a bisection search to find the maximally large perturbations y^* from $\tilde{y}(t)$ that can be included in $\mathcal{D}|_y$.

The values of the dominance strengths will remain approximately unchanged under these perturbations provided the input variables to the differential equation for y do not change significantly. Herein lies the benefit of defining the dominance strengths in Eq. 2.4 for Ψ to be independent of the instantaneous value of y , and dependent instead on y_∞ . The position of y_∞ depends directly on the values of the inputs in Γ_y only, and not on y . Therefore it is sufficient to verify three conditions on the inputs to F_y in order that the actives set remains unchanged after a perturbation $\tilde{y}(t_s) \rightarrow y^*(t_s)$:

- Fast inputs $x \in \mathcal{F}_{y,\gamma}(t_s)$, which almost instantaneously reach perturbed values $x^* \approx x_\infty(y^*)$, must not cause a change in $\mathcal{A}_{y,\varepsilon}(t_s)$ when it is recomputed using the perturbed values x^* . This is checked for both the active *and* the inactive inputs, to avoid introducing a shadowing error. Furthermore, a global check can be made to ensure that these changes in x do not change *any* $\mathcal{A}_{z,\varepsilon}(t_s)$ in the system, for $z \neq x$.
- Slow inputs $x \in \mathcal{S}_{y,\gamma}$ are assumed not to change at all under the perturbation, on the local time scale of y ’s evolution. Therefore, these will not impact the dominance strengths Ψ_x under the perturbation.
- The remaining dynamic inputs $x \in \Gamma_y$ have an $\mathcal{O}(1)$ time scale (i.e. are considered neither fast nor slow). How x responds to the perturbation in y depends on whether y is currently in *its* active set, $\mathcal{A}_{x,\varepsilon}$ (among other things). If this is so, then y_∞ must be re-evaluated with the orbits $\tilde{x}(t)$ replaced with new estimates for the $x(t)$ following the perturbation. In the absence of a more sophisticated method to ensure that these estimates will be safe, we assume the worst-case scenario: namely, that x is as far from $\tilde{x}(t)$ as possible. This

means we estimate $x(t) = x_\infty(t)$, evaluated at y^* . The active set for y can then be re-evaluated using the perturbed y_∞ , and tested for change. If $y \notin \mathcal{A}_{x,\varepsilon}$, then DSSRT estimates that x will not change significantly on the local time scale.

Finally, DSSRT tests whether the inputs have changed their membership in the sets $\mathcal{S}_{y,\gamma}(t_s)$ and $\mathcal{F}_{y,\gamma}(t_s)$, by re-determining these sets using the τ_y and τ_x values evaluated at the perturbed values y^* and x^* .

2.12. Bifurcations in the regime models. Reduced regimes can be studied for the loss of stability of any fixed points that exist in the local model, as parameters change (including the quasi-static parameters defined earlier). The loss of stability of periodic orbits requires global arguments which are not developed here, although the breaking of certain types of regime validity condition could be used as an indication that a constructed or perturbed orbit is diverging from a reference limit cycle orbit. As a parameter is varied, a sign change in τ_x indicates that x_∞ has switched between being an attractor and a repeller. This is conceptually similar to the occurrence of a local bifurcation, when x_∞ is viewed as an ‘instantaneous fixed point’ and τ_x is interpreted as an associated ‘instantaneous eigenvalue’ (§2.8).

The structure of the regimes could also be used to set up a more conventional bifurcation analysis, either by hand, such as that undertaken in [57], or using a numerical continuation software package such as AUTO [13]. Examples of local bifurcation analysis using the regimes are given in §4.4 for a Hodgkin–Huxley model neuron.

3. Application to a Hodgkin–Huxley model neuron.

3.1. A synaptically-driven Hodgkin–Huxley neuron. The example ODE system studied for the remainder of this paper models a Hodgkin–Huxley-type neuron with a single inhibitory chemical synapse as an external input. In a traditional form of notation, the system of equations consists of the following current-balance equation for the membrane potential V , and the associated equations for the non-dimensional activation variables $x(t) \in [0, 1]$:

$$\begin{aligned} C \frac{dV}{dt} &= I_{\text{ionic}}(V, m, h, n) + I_{\text{external}}(V, t) \\ &\equiv \bar{g}_m m^3 h (V_m - V) + \bar{g}_n n^4 (V_n - V) \\ &\quad + \bar{g}_l (V_l - V) + \bar{g}_s s (V_s - V) + I_b, \end{aligned} \tag{3.1}$$

$$\tau_x(V) \frac{dx}{dt} = x_\infty(V) - x, \quad x = m, h, n, \tag{3.2}$$

where we define the internal ionic current $I_{\text{ionic}} = \bar{g}_m m^3 h (V_m - V) + \bar{g}_n n^4 (V_n - V) + \bar{g}_l (V_l - V)$, the sum of a fast sodium current, a fast potassium current, and a ‘leak’ current. m represents the sodium channel activation in the cell membrane, h is the sodium channel inactivation, and n is the potassium channel activation. The external current $I_{\text{external}} = \bar{g}_s s (V_s - V) + I_b$ is the sum of a synaptic input and a fixed bias current. I_{ionic} is the source of the membrane’s excitability; in other words, its ability to generate ‘action potential’ spikes. The timing of spikes is dictated by I_{external} when all other parameters are fixed. The coefficients \bar{g}_x represent the maximum conductances of the ionic channels. Each activation variable has a voltage-dependent time scale $\tau_x(V)$ and instantaneous asymptotic target $x_\infty(V)$, which are explicitly known functions. The standard choice of $C = 1 \mu\text{F}/\text{cm}^2$ for this type of cell leads us to drop the capacitance parameter from our equations hereafter. In this example, the values for all the parameters and functions $\tau_x(V)$, $x_\infty(V)$ are fixed, and are detailed in the Appendix.

The synaptic drive input has a gating variable $s(t) \in [0, 1]$, which is the fifth variable in the system. It has a similar form to an activation variable:

$$\frac{ds}{dt} = \alpha \Theta(V_{\text{pre}}(t)) (1 - s) - \beta s, \tag{3.3}$$

where $\Theta(V_{\text{pre}}) = (1 + \tanh(V_{\text{pre}}/4))/2$ is a smooth step function, and α and β control the rise and fall times of an inhibitory pulse. Here, the inhibitory pulse is stimulated by a pre-synaptic

spike from an externally applied, time-varying input, $V_{pre}(t)$ (defined in the Appendix), that mimics the regular spiking of another cell. By choosing the reversal potential V_s in Eq. (3.1) to be below the threshold of spike initiation, this synaptic input is inhibitory.

3.2. Inputs to the voltage equation. We take several steps in order to standardize our notation and apply the dominant scale method. Firstly, we ignore the physiological distinction of ‘ionic’ versus ‘external’ currents to the neuron. We define $\bar{n} = \bar{g}_n$, $\bar{l} = \bar{g}_l$, $\bar{s} = \bar{g}_s$, and $\bar{b} = I_b$. These re-labelings are superficial, but we make the leak and bias current terms consistent with the notation of other inputs by formally including the gating ‘variables’ $l \equiv 1$ and $b \equiv 1$, respectively. For the sodium conductance, we consider m to be the primary variable and h the auxiliary (i.e. a modulator of m). As a result, we will not analyze the effect of perturbations in h . This choice of primary variable is satisfactory (although somewhat arbitrary) because both variables depend only on V , and not on any external sources. We therefore define the *time-varying* maximal conductance $\bar{m} = \bar{m}(t) = \bar{g}_m h(t)$, and henceforth write the sodium current $\bar{m}m^3(V_m - V)$.

It is appropriate to consider all additive terms that contribute to the r.h.s. of Eq. (3.1) as inputs because each term has a distinct physiological interpretation. Thus, for the voltage equation, the five input terms are the sodium activation/inactivation term $\bar{m}m^3(V_m - V)$, the potassium activation term $\bar{n}n^4(V_n - V)$, the leak term $\bar{l}(V_l - V)$, the synaptic term $\bar{s}s(V_s - V)$, and the bias current $\bar{b}b$. The five corresponding variables form the set of inputs $\Gamma_V = \{m, n, l, b, s\}$, where we include only primary variables.

The variables m , h , n , and s , are governed by their own differential equations, and so the inputs to Eq. (3.1) that involve them are dynamic inputs. The leak and bias current inputs are passive. In addition to this distinction, we note that an input term is either explicitly dependent on V , having the form $\bar{x}x^{q_x}(V_x - V)$, or independent, having the form $\bar{x}x^{q_x}$. Here, \bar{x} is the maximal value of the input (time-varying in the presence of auxiliary variables), $x \equiv x(t) \in [0, 1]$ determines the time-course of the input, and q_x is a positive integer. Inputs of the first type belong to Γ_1 , and those of the second type belong to $\Gamma_2 = \Gamma_V \setminus \Gamma_1$.

Using these definitions, a simple algebraic manipulation shows that the voltage and synaptic equations have the same form as the activation variables:

$$\tau_V(\{x\}_{x \in \Gamma_1}) \frac{dV}{dt} = V_\infty(\{x\}_{x \in \Gamma_V}) - V, \quad (3.4)$$

$$\tau_s(V_{pre}) \frac{ds}{dt} = s_\infty(V_{pre}) - s, \quad (3.5)$$

where

$$\begin{aligned} 1/\tau_V &= \bar{m}m^3 + \bar{n}n^4 + \bar{l}l + \bar{s}s, \\ V_\infty &= (\bar{m}m^3V_m + \bar{n}n^4V_n + \bar{l}V_l + \bar{s}sV_s + \bar{b}b) \tau_V, \\ \tau_s &= \alpha\Theta(V_{pre}) + \beta, \\ s_\infty &= \alpha\Theta(V_{pre}) / (\alpha\Theta(V_{pre}) + \beta). \end{aligned}$$

3.3. Conditionally linear ODEs. As a result of the re-arrangement of the HH system, we see that each equation of the system explicitly has the form $\tau_x \dot{x} = x_\infty - x$, where $x = V$, m , n , h , or s . τ_x and x_∞ may be functions of external inputs or other variables in the system (but not of x). Also, each $x_\infty(t)$ is unique. These are general properties of Hodgkin–Huxley-type models, due to the *conditional linearity* of the equations, i.e. that each differential equation is linear in its own dependent variable, when the values of the other variables appearing in the equation are known. The conditional linearity of the HH model simplifies various computations and checks required by our method. For instance, because the characteristic time scale coefficients τ_x are explicitly known functions that are strictly positive, we observe that the HH system is dissipative at all times. Another beneficial consequence of conditional linearity is that each variable x is attracted to $x_\infty(t)$ *exponentially*, which is a stronger property than the normal hyperbolicity that we require.

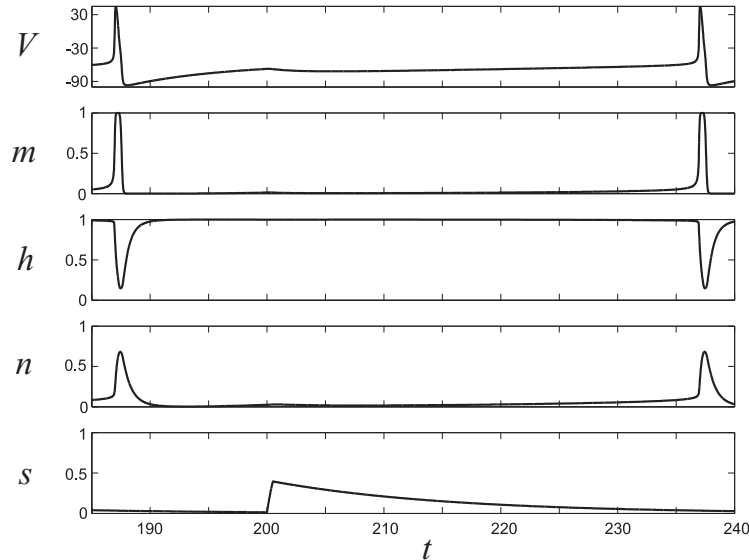


FIG. 3.1. *The limit cycle for the HH system projected in its 5 constituent dimensions.*

3.4. Dominance strengths. In this model of a single neuron we consider only the influence of inputs on the V dynamics, because the other equations have only one input. There are two types of influence that inputs have on the differential equation for V . Inputs in Γ_1 affect both the V_∞ and τ_V values, whereas those in Γ_2 affect only V_∞ . Because of the conditional linearity of the HH equations, and the positivity of the activation variables x , their time scales τ_x , and their powers q_x , the definition of dominance strength in Eq. (2.4) reduces to a form that is computationally more practical.

$$\Psi_x(t) = \begin{cases} \tau_V(t) q_x \bar{x} x^{q_x}(t) |V_x - V_\infty(t)| & \text{if } x \in \Gamma_1, \\ \tau_V(t) q_x \bar{x} x^{q_x}(t) & \text{if } x \in \Gamma_2. \end{cases} \quad (3.6)$$

We see that for Γ_1 inputs, Ψ_x resembles the input term for x (in physiological terms, this would be the current through the channel associated with x) except that V_∞ replaces V , and there is an additional multiplication by τ_V . For Γ_2 our definition coincides with the associated input term (modulo the factor of τ_V).

3.5. Local epoch models. For any initial condition, the HH system quickly settles to a limit cycle (shown in Fig. 3.1), having the same period as the inhibitory driving signal, namely 50 ms (hereafter denoted T). This limit cycle, and a neighborhood around it, will be the focus of the subsequent analysis, and we denote it $\tilde{\mathbf{X}}(t)$, where $\tilde{\mathbf{X}} = (\tilde{V}, \tilde{m}, \tilde{n}, \tilde{h}, \tilde{s})$ defines its components.

Focusing on the voltage V , the epoch model in a neighborhood of $\tilde{\mathbf{X}}(t)$ over $t \in [t_p, t_{p+1})$ is given by

$$\frac{dV}{dt} = \sum_{x \in \hat{\Gamma}_1(t)} \bar{x} x^{q_x} (V_x - V) + \sum_{x \in \hat{\Gamma}_2(t)} \bar{x} x^{q_x}, \quad (3.7)$$

$$\left\{ \frac{dx}{dt} = \frac{1}{\tau_x} (x_\infty - x) \right\}_{x \in (\hat{\Gamma}_1 \cup \hat{\Gamma}_2)(t)}, \quad (3.8)$$

where $\hat{\Gamma}_1(t) = \mathcal{A}_{V,\varepsilon}(t) \cap \Gamma_1$, $\hat{\Gamma}_2(t) = \mathcal{A}_{V,\varepsilon}(t) \cap \Gamma_2$, and the equation for the auxiliary variable h is also included whenever $m \in \hat{\Gamma}_1(t)$.

Using $\varepsilon = 2/5$ in DSSRT we obtained an epoch sequence of length 12. The sequence is tabulated in the first three columns of Table 3.1. (Values $\varepsilon \in [1/5, 1/3]$ have yielded reasonable results for the

Epoch	Time interval	$\mathcal{A}_{V, \varepsilon}$	$\mathcal{P}_{V, \varepsilon}$
1	[00.00, 00.03)	s, b, l	m, n
2	[00.03, 28.26)	s, b	m, n
3	[28.26, 29.04)	s, b, l	m, n
4	[29.04, 33.57)	m, s, b, l	n
5	[33.57, 34.59)	m, b, l	s, n
6	[34.59, 34.77)	m, l	s, n
7	[34.77, 36.87)	m	s, n
8	[36.87, 37.62)	m, n	
9	[37.62, 38.79)	n	m
10	[38.79, 39.00)	n, b	m, s
11	[39.00, 39.21)	n, b, l	m, s
12	[39.21, 49.98)	b, l	m, n, s

TABLE 3.1

The epoch sequence determined by DSSRT for the limit cycle oscillation, with period $T = 50$ ms. Time intervals are measured relative to the onset of an inhibitory pulse at $t = 200$ ms. The size of the numerical integration step and the re-sampling done by DSSRT caused the final interval to stop short of precisely $t = T$.

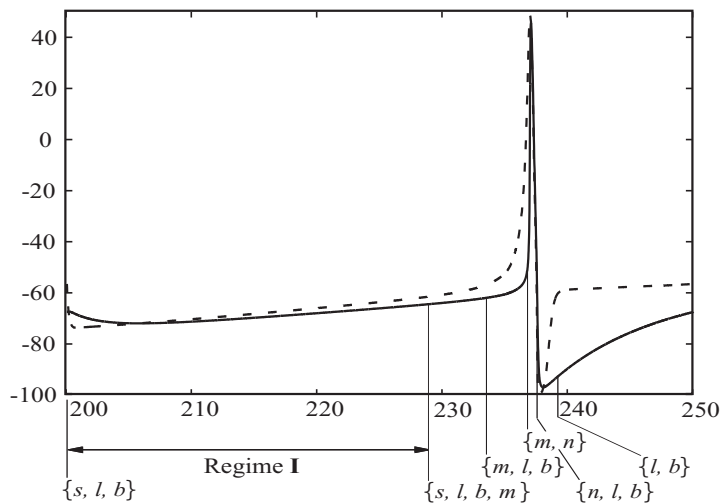


FIG. 3.2. One period in $\tilde{V}(t)$, with $V_\infty(t)$ (dotted line). The reduced set of regimes along the limit cycle are shown below the graph with their associated set of actives $\mathcal{A}_{V, \varepsilon}$.

neural models we have studied so far.) A temporal resolution of 0.03 ms was used to analyze the numerically integrated orbit (computed using the Runge–Kutta scheme at a time step of 0.01 ms). This resolution accounts for the slight discrepancy of 0.02 ms in the total length of the regimes making up the cycle from the known driving period of 50 ms, despite having used initial conditions for the system very close to the periodic orbit. The temporal resolution of DSSRT’s analysis can be altered by the user to match the smallest time scales of the events in the dynamics.

3.6. Potentially active inputs. Another consequence of conditional linearity aids the calculation of potentially active inputs. For such systems, the value of the input variable that maximizes its dominance strength can be determined explicitly as a function of the system state. The turning-point condition $d\Psi_x/dx = 0$ can be solved explicitly from the r.h.s. of Eq. (3.6), and DSSRT takes the maximum value of the dominance strength evaluated at the solutions to this turning point condition and at the end points of the assumed bounds for the variable x (i.e. 0 and 1 for the activation variables in the HH system). This approach avoids the need to calculate the second derivative of the dominance strength to check for a maximum. The potentially active variables in each epoch along the periodic orbit $\tilde{\mathbf{X}}(t)$ for the HH system are tabulated in the final column of Table 3.1.

Reg.	Time interval	Epochs	Dynamic	Passive	Bif. par.	Dim.
I	[00.00, 29.04)	1, 2, 3	s, V	l, b	m	2
II	[29.04, 33.57)	4	$m[\text{F}], h, s, V$	l, b		3
III	[33.57, 36.87)	5, 6, 7	$m[\text{F}], h, V$	l, b	n	2
IV	[36.87, 37.62)	8	$m, h[\text{S}], n[\text{S}], V$			2
V	[37.62, 39.21)	9, 10, 11	n, V	l, b		2
VI	[39.21, 49.98)	12	V	l, b	s	1

TABLE 3.2

The six regimes determined by DSSRT: [F] indicates ‘fast’ variable response, [S] indicates ‘slow’. Also shown: the half-open intervals marking the temporal extent of the regimes (relative to the onset of an inhibitory pulse at $t = 200$ ms); the epochs included in the regime; the dynamic and passive variables in $\mathcal{A}_{V, \varepsilon}$; quasi-static bifurcation parameters for the regime; the effective dynamic dimension of the regime.

3.7. Reduced dynamical regimes. Six regimes were calculated for the HH system using $\gamma = 1/3$, which are shown in Table 3.2 and Fig. 3.2. We will denote these regimes by $R_{\mathbf{I}} - R_{\mathbf{VI}}$. We see that the dynamics along most of the orbit is effectively two-dimensional (although from regime to regime these are generally different dimensions). This means that phase-plane techniques can be used to do bifurcation analysis [26, 32]. During a spike m, h and n play the most dominant roles, as expected. This is captured by regimes $R_{\mathbf{III}}$ through $R_{\mathbf{V}}$. $R_{\mathbf{IV}}$ exactly corresponds to the two-dimensional asymptotic analysis of Hodgkin–Huxley excitability in [61] (also see §4.4). $R_{\mathbf{VI}}$ and $R_{\mathbf{I}}$ demonstrate the validity of a linear one-dimensional membrane model (e.g. the leaky integrate-and-fire model [36, 46]) with external synaptic input, for the non-refractory and non-spiking part of the dynamics.

4. Analysis of the reduced models.

4.1. Approximating the periodic orbit. We tested the accuracy in constructing an approximation to the periodic orbit $\tilde{V}(t)$, by numerically integrating the piecewise-switched systems (3.7)–(3.8) over one period, using the initial conditions $\tilde{\mathbf{X}}(t_1)$. While neither a quantitative nor rigorous test of accuracy, it can be seen in Fig. 4.1 that the orbits are qualitatively very similar, and in particular the action potential spikes occur with a time difference of less than 1 ms. (As a result of small differences in the variable values of the full and reduced models, at the times when m and n become active and inactive, the reduced model spike is slightly misshapen.) The construction of this orbit was naïve, because for simplicity we used the epoch-switching times $\{t_p\}$ calculated from $\tilde{\mathbf{X}}(t)$, rather than determining these times self-consistently for the constructed orbit during its evolution. An algorithm to construct orbits from an initial condition appropriately, using the reduced models, is still in development (§2.11). However, the fact that the constructed orbit shown is very near to $\tilde{\mathbf{X}}(t)$ demonstrates that piecewise use of the local models does not cause accumulation of error in the orbit through time. A heuristic explanation of why this is true was given in §2.11.

Due to the emerging strong separation of dominance scales during a spike, the automatically generated regimes are not sensitive to changes in ε or γ , provided these were chosen with some care as a result of exploratory numerical investigation. Moderate changes in these parameters may change the detailed order, constitution, and timing of the epochs in an epoch sequence, but after consolidation into the reduced dynamical regimes these differences are typically eliminated. This shows that the precise timing of regime changes appears to have little effect on the accuracy of the reduced models (especially for the purposes of investigating bifurcation scenarios).

4.2. The asymptotic target as an organizing center. During $R_{\mathbf{IV}}$, after the peak of a spike, the target V_∞ is controlled by m, h , and n . All of these variables have time scales at least twice as long as τ_V at this point, and so for the remainder of the spike V_∞ is a good approximation to V . In this regime the dynamics resemble singularly perturbed dynamics where the target is a slow invariant manifold (that is attracting in all directions). This is not easy to visualize in Fig. 4.2, where it appears that V is moving alongside V_∞ at an equal velocity. However, perturbed V orbits integrated numerically during that regime relax extremely quickly toward $V_\infty(t)$. This situation

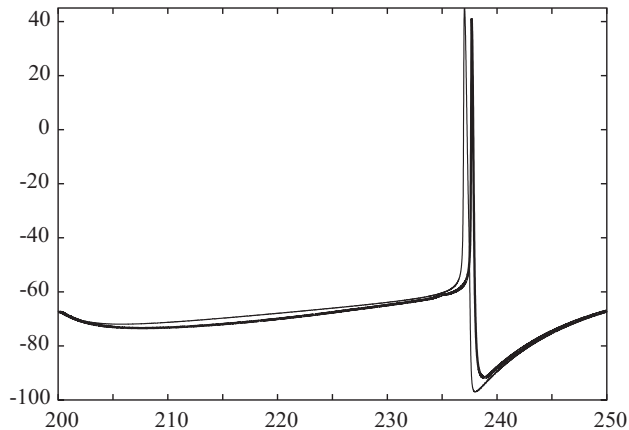


FIG. 4.1. The periodic orbit $\tilde{V}(t)$ (thin line) compared to an orbit computed by piecewise application of the local models specified by $\mathcal{A}_{V, \varepsilon}(t)$ (thick line).

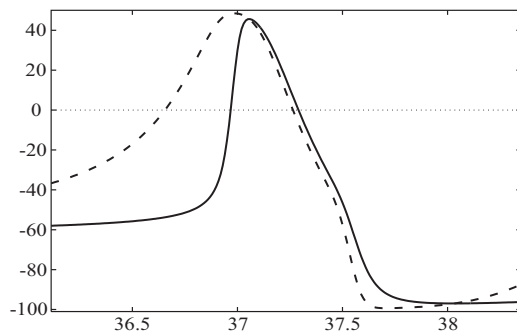


FIG. 4.2. $V_\infty(t)$ (dotted line) and $\tilde{V}(t)$ during an action potential spike. Time is indicated relative to the onset of an inhibitory pulse.

is reflected by the large domain of validity for this regime, which is determined in the next section and plotted in Fig. 4.3.

Because the free parameters ε and γ are not necessarily small, the attraction toward the asymptotic target is not always fast in every direction, so that the target may not represent a good approximation to the actual motion. For instance, in $R_{\mathbf{VI}}$ the transient decay of V toward V_∞ is shown in Fig. 3.2 to occupy the entire regime. Nonetheless, $\tilde{\mathbf{X}}_\infty$ *always* provides information about the direction of response of the system to a range of perturbations or parameter variations that do not violate the validity conditions for the regimes, and the time scale of the variables indicate the rate of their return toward this target. In this sense, therefore, $\tilde{\mathbf{X}}_\infty(t)$ organizes the local dynamics.

4.3. Regime validity conditions. For the limit cycle $\tilde{\mathbf{X}}(t)$, the restricted d.o.v. $\mathcal{D}(2/5, 1/3)|_V$ was estimated by DSSRT, and the result is plotted in Fig. 4.3. A range of orbits for the full Hodgkin–Huxley system were computed numerically, having V initial conditions inside this set, while the other variables' initial conditions were taken from the reference orbit $\tilde{\mathbf{X}}(t)$. The computed orbits were found to undergo the sequence of structural changes prescribed for the reference orbit. As expected, the duration of the computed orbits in each regime varied according to the degree of perturbation that the initial condition had undergone relative to the reference orbit at the corresponding time. The d.o.v. qualitatively retains its shape if γ is varied, but tends to shrink slightly as this parameter is decreased. Observe that $\mathcal{D}|_V$ is very narrow during $R_{\mathbf{III}}$ and $R_{\mathbf{IV}}$. In this region the spiking time of a Hodgkin–Huxley model neuron is well known to be sensitive to perturbations. Also observe that during the non-spiking regimes the d.o.v. remains below $V \approx -64$ mV,

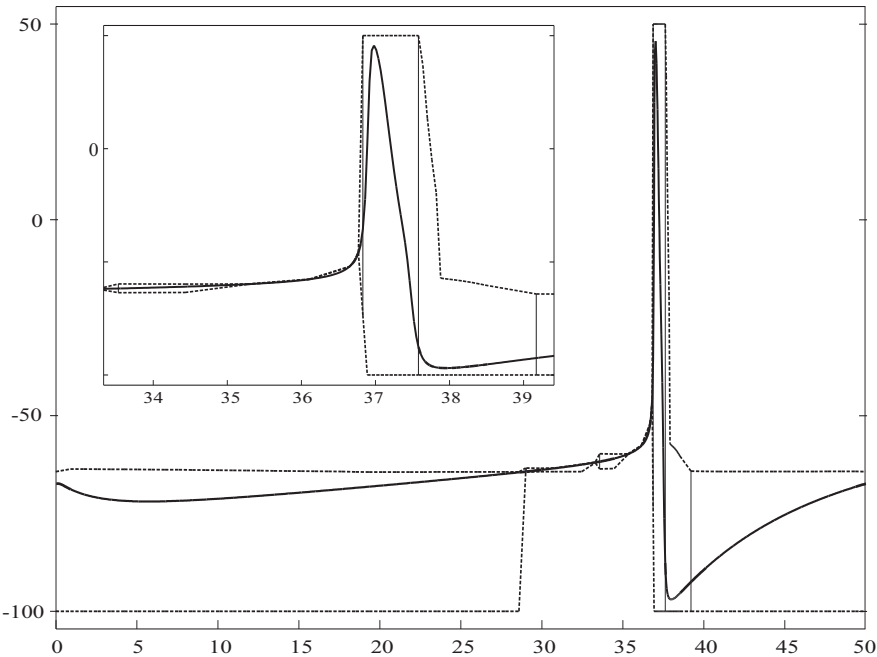


FIG. 4.3. A projection onto the variable V of the domain of validity for the reduced regimes is shown between the dotted lines. The thick solid line indicates the periodic orbit $\tilde{V}(t)$. Thin vertical lines indicate events that separate regimes (e.g. shown at $t \approx 37.7$ and 39.2). The inset shows a close-up during regimes $R_{\text{III}}-R_{\text{V}}$. The d.o.v. has been truncated at $V = 50$ mV and -100 mV, at the user-specified maximum and minimum bounding values for V . Time is indicated relative to the onset of an inhibitory pulse.

which effectively defines the ‘spiking threshold’ [40]. Orbits started above this point immediately joined a regime where m is strongly dominant, and a spike was elicited shortly afterward.

The strongly dissipative nature of the HH system is also exhibited by the large d.o.v. in V during a spike ($37 < t < 38$) and immediately after the onset of the inhibitory pulse ($0 < t < 29$). This is shown by the vertical extent of the dotted lines surrounding $\tilde{\mathbf{X}}$ during these times in Fig. 4.3. In both cases the extent reaches the minimum user-specified bound on V at -100 mV, and during the spike it also reaches the maximum bound at 50 mV, at which point DSSRT ceases to extend the d.o.v. further. If the bounds had not been imposed the d.o.v. would extend much further into a range of non-physiologically realistic voltages.

4.4. Bifurcations and regime change conditions. During an action potential spike (R_{IV}) the local model exhibits bi-stability. The regime’s phase-plane model is in the variables (V, m) , which has three fixed points at the beginning of the regime. This situation is shown in Fig. 4.4, which is based on graphical output generated by DSSRT. Fixed point 2 is unstable, the others are stable. The system begins the regime near the unstable fixed point in the basin of attraction of fixed point 3. The V nullcline is controlled by the quasi-static motion of h and n . As these quantities are varied through the remaining course of the spike (according to $\tilde{h}(t)$ and $\tilde{n}(t)$), the system undergoes a saddle-node bifurcation, eliminating the nearby stable fixed point and swiftly moving the system toward the remaining fixed point, which is near the reversal potential for the n variable. Estimating the values of the dominance strengths as this fixed point is approached predicts the point at which m is no longer an active variable, and hence when the model of the local dynamics should be passed to R_{V} .

Not all structural changes in the system along an orbit are related to local bifurcations in the regimes’ reduced models. In R_{I} , after the onset of an inhibitory pulse, a slow-moving attracting point exists in the local model. It moves slowly as the inhibitory input variable s decays. As V tends slowly toward this point along a constructed orbit in the reduced system, the value of m varies slowly because m is sensitive to changes in V along the reference limit cycle $\tilde{\mathbf{X}}(t)$. For

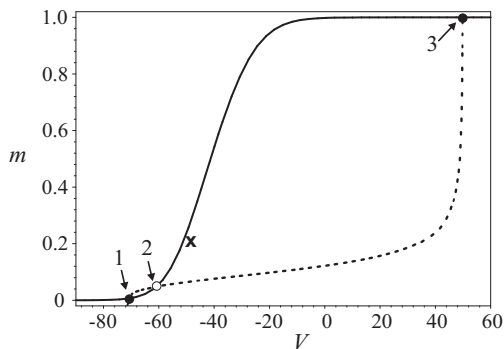


FIG. 4.4. The (V, m) phase plane of R_{IV} , showing the two nullclines at the beginning of the regime, the three fixed points and the regime's initial condition marked by a cross. The V -nullcline is the dotted line.

instance, it can be seen from the third column of Table 3.1 that m is *potentially* active throughout R_I , and that it does become active in the next regime. Therefore, because m is not explicitly modeled in R_I , it must be tracked in order to avoid a shadowing error, and to pass control to the next regime at the correct point. This explains why m is set as a quasi-static bifurcation parameter. DSSRT determines that the time scale of m is fast with respect to V in R_I , so that $m \approx m_\infty$, which is an explicitly-known function of V . At some point during the construction of an orbit in R_I , the un-modeled m variable increases to a value that results in it joining the active set $\mathcal{A}_{V,\varepsilon}$. This point can be determined by continual re-calculation of the dominance strengths along the evolving orbit, evaluating Ψ_m using the approximated value of m . Thus we have self-consistently determined the point of transition to R_{II} as being a violation of the domain of validity of R_I . Referring back to the domain of validity $\mathcal{D}|_V$ shown in Fig. 4.3, we see that during R_I the upper limit of the d.o.v. estimates the ‘spiking threshold’ of the cell. This marks the extent of the permissible depolarization of constructed V orbits relative to $\tilde{V}(t)$, after which point m becomes activated and the regime’s assumptions are violated.

5. Discussion.

5.1. Summary of results. We have presented an automatic method designed to aid the analysis of high-dimensional ODE systems possessing multiple scales, in a way that complements numerical simulation and intuitive reduction methods. Our method has been developed into a MATLAB code named DSSRT, which establishes reduced regimes for a system quickly and with near autonomy, without the artificial introduction of small parameters into the equations or explicitly non-dimensionalizing them.

With only minimal initial specification of the ODE system and the limit cycle to DSSRT, and the selection of two free parameters, the software tool resolved the dynamical processes underlying an orbit of a synaptically-driven Hodgkin–Huxley (HH) model neuron. The HH model is a 5-dimensional, stiff, and nonlinear ODE system, involving pulsatile forcing and changing time scale relationships. DSSRT generated a set of reduced dynamical regimes of low dimension within which bifurcation and perturbation analyses can be performed. A major benefit of the dominant scale method is that it provides a *quantitative* estimate of the domain of validity for each regime (both in time and with respect to perturbations from the limit cycle), without using numerical shooting methods. In our application to the HH model, DSSRT’s conservative form of the regime validation process developed in §2.11 yielded a reasonably accurate domain of validity (§4.3).

The dominant scale method also provides a computational tool for characterizing multiple time scales, as we demonstrated for a van der Pol oscillator that was not close to the singular limit. This tool allows DSSRT to automatically reduce such systems to the familiar slow-fast subsystems, and to efficiently estimate the behavior of the system in a neighborhood of a stable limit cycle. Furthermore, the domain of validity calculation estimates the extent of this neighborhood.

5.2. Related work. The method presented complements work undertaken by the same authors [57]. In that work we rigorously construct a limit cycle describing sub-threshold oscillations and spiking for a seven-dimensional biophysical model of an entorhinal cortex spiny stellate cell. We do so by asymptotically reducing the model to a sequence of two-dimensional regimes. Each one is then analyzed by applying geometric phase-plane techniques. The regimes are derived formally by identifying active and inactive currents in terms of their relative size, in an analogous fashion to the comparison of the Ψ_x quantities used here. DSSRT uses two explicit thresholds for distinguishing small scales (ε and γ), whereas in [57] scale separations are determined self-consistently during the asymptotic analysis of each regime. Application of DSSRT to the stellate cell model produced consistent results. The analytical techniques used there to construct the periodic orbits will form the basis of an extension of DSSRT that will permit it to analytically construct approximations to limit cycles and more complex orbits. Additionally, in [9] a single HH neuron without synaptic input was analyzed and reduced to a set of regimes that is consistent with previous formal analyses of the HH equations [38, 60, 61], providing further validation of our method.

Algorithmic techniques for the dimension reduction of high-dimensional dynamical systems exist elsewhere, from the data analysis of time-series [33, 55], to Model Order Reduction (MOR) methods for control systems [4, 56], to partitioning and ‘lumping’ methods for large chemical systems that focus on multiple time scales with explicit small parameters [10, 12, 20, 21, 47]. These techniques tend to focus on non-oscillatory dynamics, with long-term behavior governed by fixed points. Also, they tend to focus on separations in *time* scale only. MOR methods generally involve projecting the dynamics to lower-dimensional subspaces that optimally span data sets obtained from numerical simulation or experiments [54]. The projections maximize the amount of ‘statistical energy’ in the subspace, but the projected ‘modes’ are not necessarily those of most importance to the dynamics [59]. This is because a primary goal of the MOR method is to increase the computational efficiency of solving very large-scale models (e.g. $N > 1000$), rather than trying to explore the fine dynamical structure underlying complex dynamics of moderate-sized models.

5.3. Applications. An immediate application of the dominant scale method is to gain intuition about detailed physiological ODE models. The current focus on conditionally linear ODE systems simplifies the algorithms needed by DSSRT by taking advantage of the explicit representation for the asymptotic targets and characteristic time scales. This makes DSSRT’s application ideal for neuro-physiological models, which generally take conditionally linear form. For problems requiring models to be fitted to experimental data or other constraints, we aim to add features to DSSRT that will support parameter estimation for existing models. Furthermore, similar features would allow the desired bifurcation scenarios to be designed into new models of a phenomenon.

We believe our methods are applicable to a much wider domain of ODE systems. To deal with non-conditionally linear systems, for instance, the principal quantities needed in our analysis may need to be calculated numerically, or they could be determined implicitly using automatic differentiation techniques [23, 27]. So-called ‘hybrid’ dynamical systems are another class of system that our method is well suited to. Hybrid systems are characterized by interactions between continuous dynamics and discrete events [5, 24, 30, 65], and have a wide variety of applications. Their structure is based on differential-algebraic systems [62]. Model constraints determine when events happen based on the system’s state. The occurrence of an event means a discrete change is made to the equations of the system. Together, these events define a set of piecewise-switched local models of the full system, closely resembling the sequences of reduced regime models that we derive in this paper. It would be interesting to explore the integration of established computational methods for hybrid systems [6, 7, 63] with our method.

If the correctness of our method can be rigorously proved, DSSRT will provide a framework for undertaking computer-assisted proofs about the properties of some ODE systems. In the meantime, we would like to better understand the observed accuracy of the reduced models that DSSRT calculates, in relation to the assumed characteristics of the equations being studied. For instance, the HH system is globally dissipative (often strongly), and we suspect that this is the reason for the low accumulation of error in constructing local orbits, as transitions are made

between reduced models. However, we believe that the reliability of our method is maintained if there is *some* expansion present in the vector field under investigation, particularly if it is limited in temporal duration.

Additionally, we envision application of the dominant scale method to discrete time (possibly stochastic) systems, in particular to time-series analysis. If the underlying difference or differential equations are not known explicitly, but are instead estimated using a set of local flow data [1, 19], then our techniques could provide a new dynamical systems-oriented approach to nonlinear system estimation problems.

5.4. Toward a global dominant scale analysis. At present, the dominant scale method focuses on one variable of a system at a time. For this variable, a set of piecewise regime models for the system near a known orbit can be generated, with an associated domain of validity. This situation is adequate to construct and analyze *local* properties of orbits that remain sufficiently close to their counterparts in the reference orbit $\tilde{\mathbf{X}}(t)$. However, the domains of validity are estimated in a conservative manner partly because the method does not generate *globally valid* information about the propagation of changes to all the variables at once. Instead, we estimated the propagation of perturbations through one coupled variable at a time, assuming the remainder were unchanged from the reference orbit. The benefit of this approach is greater computational efficiency.

Our method could be extended to account for the global changes that result from trying to construct orbits which diverge from the reference orbit. A more sophisticated approach to building the reduced regimes and their d.o.v.'s would be necessary—one that permits the dominant scale analysis to be focused on multiple variables simultaneously. Fortunately, for the Hodgkin–Huxley example system studied in §3 and §4 it was unnecessary to perform a global dominant scale analysis using all the system's variables: only one of the right-hand sides have more than one input term.

In the absence of a globally-based method, DSSRT does not currently support the automatic construction of orbits or the focusing of the method on multiple variables of interest. The additional complexity in automatically determining the necessary self-consistency conditions, as discussed in §2.11 and §4.4, remains a topic for future study. The inclusion of an inhibitory external input to the neuron studied here foreshadows the automated treatment of networks of neurons, such as those involving mutual inhibition. In such networks, the external input modeled here would be driven by another neuron. The mechanisms of mutual inhibition [8, 28, 66, 67] are of great interest, being important features of many neural rhythms [42, 43, 58, 68, 69]. A type of global self-consistency analysis has been undertaken by hand in the study of the fine structure underlying inhibitory-based neural rhythms [16, 35]. Although these methods were developed in an *ad hoc* way for specific neural models, they employ powerful assumptions about multiple-scale dynamics in general. These assumptions motivate our present and future study into more formalized, general purpose tools for analyzing coupled ODE systems.

Appendix. Activation functions and parameters for the Hodgkin–Huxley model.

For the HH model we define $\tau_x = \alpha_x + \beta_x$ and $x_\infty = \alpha_x / (\alpha_x + \beta_x)$ for each of $x = m, h, n$ in Eqs. (3.2), using the following forward and backward activation rates.

$$\begin{aligned}\alpha_m(V) &= 0.32 (V + 54) / \left(1 - e^{-(V+54)/4}\right) \\ \beta_m(V) &= 0.28 (V + 27) / \left(e^{(V+27)/5} - 1\right) \\ \alpha_h(V) &= 0.128 e^{-(50+V)/18} \\ \beta_h(V) &= 4.0 / \left(1 + e^{-(V+27)/5}\right) \\ \alpha_n(V) &= 0.032 (V + 52) / \left(1 - e^{-(V+52)/5}\right) \\ \beta_n(V) &= 0.5 e^{-(57+V)/40}\end{aligned}$$

The external voltage signal $V_{pre}(t)$ is modeled as a rectangular pulse, having duration 0.5 ms, a baseline at -80 mV, and a maximum of 30 mV. Its period is 50 ms. This pulse is designed to

have an almost identical driving effect on the synaptic response equation (3.3) as a real action potential spike, by fitting its area and duration.

We use the following parameter set throughout the paper.

$$\begin{array}{llllll} \bar{g}_m = 100 & \bar{g}_n = 80 & \bar{g}_i = 0.1 & \bar{g}_s = 0.8 & \alpha = 1 & \beta = 0.067 \\ V_m = 50 & V_n = -100 & V_i = -67 & V_s = -80 & I_b = 1.3 & C = 1 \end{array}$$

The units of conductance are mS/cm², those of potential are mV, those of current are μ A/cm², and those of capacitance are μ F/cm².

Acknowledgements. This work was supported by NSF grants DMS-0211505 and DMS-9706694, and by the Burroughs Wellcome Fund award 1001749. Thanks go to Tasso Kaper, John Guckenheimer, Steve Epstein, and Elisabeth Kingsbury, for helpful comments and discussion. We also thank the referees for their valuable suggestions.

REFERENCES

- [1] H. D. I. ABARBANEL, *Analysis of Observed Chaotic Data*, Springer, 1996.
- [2] L. F. ABBOTT AND T. B. KEPLER, *Model neurons: from Hodgkin-Huxley to Hopfield*, vol. 368 of Lecture notes in Physics, Springer-Verlag, 1990, pp. 5–18.
- [3] C. D. ACKER, N. KOPELL, AND J. A. WHITE, *Synchronization of strongly coupled excitatory neurons: Relating network behavior to biophysics*, J. Comp. Neurosci., 15 (2003), pp. 71–90.
- [4] A. C. ANTOULAS AND D. C. SORESENSEN, *Approximation of large-scale dynamical systems: An overview*, Int. J. Appl. Math. Comput. Sci., 11 (2001), pp. 1093–1121.
- [5] M. S. BRANICKY, *Analysis of continuous switching systems: Theory and examples*, in Proc. 1994 American Control Conf., June 1994, pp. 3110–3114.
- [6] S. L. CAMPBELL, *Intelligent DAE solvers and user friendly design, simulation, and analysis packages*, in Proc. IEEE Intern. Conf. Systems, Man, and Cybernetics, 1998.
- [7] D. CHANIOTIS, M. A. PAI, AND I. A. HISKENS, *Sensitivity analysis of differential-algebraic systems using the GMRES method—application to power systems*, in Proc. IEEE Intern. Symp. Circuits and Systems, May 2001.
- [8] C. C. CHOW, J. A. WHITE, J. RITT, AND N. KOPELL, *Frequency control in synchronized networks of inhibitory neurons*, Journal of Computational Neuroscience, 5 (1998), pp. 407–420.
- [9] R. CLEWLEY, *Dominant-scale analysis for the automatic reduction of high-dimensional ODE systems*, in ICCS 2004 Proceedings, Y. Bar-Yam, ed., New England Complex Systems Institute, 2004. To appear.
- [10] P. DEUFLHARD AND J. HEROTH, *Dynamic dimension reduction in ODE models*, in Scientific Computing in Chemical Engineering, F. Keil, W. Mackens, H. Voß, and J. Werther, eds., Springer-Verlag, 1996, pp. 29–43.
- [11] C. T. DICKSON, J. MAGISTRETTI, M. H. SHALINSKY, B. HAMAN, AND A. ALONSO, *Oscillatory activity in entorhinal neurons and circuits*, Ann. N.Y. Acad. Sci., 911 (2000), pp. 127–150.
- [12] R. DJOUAD AND B. SPORTISSE, *Partitioning techniques and lumping computation for reducing chemical kinetics. APLA: An automatic partitioning and lumping algorithm*, Applied Numerical Mathematics, 43 (2002), pp. 383–398.
- [13] E. DOEDEL, H. B. KELLER, AND J. P. KERNEVEZ, AUTO, International Journal of Bifurcation and Chaos, 1 (1991), p. 493.
- [14] W. ECKHAUS, *Asymptotic Analysis of Singular Perturbations*, North-Holland, Amsterdam, 1979.
- [15] G. B. ERMENTROUT, *Type I membranes, phase resetting curves, and synchrony*, Neural Computation, 8 (1996), pp. 979–1001.
- [16] G. B. ERMENTROUT AND N. KOPELL, *Fine structure of neural spiking and synchronization in the presence of conduction delays*, Proc. Nat. Acad. Sci. USA, 95 (1998), pp. 1259–1264.
- [17] N. FENICHEL, *Persistence and smoothness of invariant manifolds for flows*, Ind. Univ. Math. J., 21 (1971), pp. 193–225.
- [18] R. FITZHUGH, *Impulses and physiological states in models of nerve membrane*, Biophysical Journal, 1 (1961), pp. 445–466.
- [19] C. W. GEAR AND I. G. KEVREKIDIS, *Projective methods for stiff differential equations: Problems with gaps in their eigenvalue spectrum*, SIAM Journal of Scientific Computing, 24 (2003), pp. 1091–1106.
- [20] A. N. GORBAN AND I. KARLIN, *Method of invariant manifold for chemical kinetics*, Chemical Engineering Science, 58 (2003), pp. 4751–4768.
- [21] A. N. GORBAN, I. V. KARLIN, V. B. ZMIEVSKII, AND S. V. DYMOVA, *Reduced description in reaction kinetics*, Physica A, 275 (2000), pp. 361–379.
- [22] J. GRASMAN, *Asymptotic Methods for Relaxation Oscillations and Applications*, Springer-Verlag, New York, 1987.
- [23] A. GRIEWANK, *Evaluating Derivatives*, SIAM, 2000.

- [24] J. GUCKENHEIMER, *Bifurcation and degenerate decomposition in multiple time scale dynamical systems*, in Nonlinear Dynamics and Chaos: Where do we go from here?, J. H. et al., ed., Institute of Physics, 2002, ch. 1.
- [25] J. GUCKENHEIMER, K. HOFFMAN, AND W. WECKESSER, *The forced van der pol equation I: The slow flow and its bifurcations*, SIAM J. Appl. Dyn. Syst., 2 (2001), pp. 1–35.
- [26] J. GUCKENHEIMER AND P. HOLMES, *Nonlinear Oscillations, Dynamical Systems, and Bifurcations of Vector Fields*, Springer-Verlag, New York, 1983.
- [27] J. GUCKENHEIMER AND B. MELOON, *Computing periodic orbits and their bifurcations with automatic differentiation*, SIAM J. Sci. Stat. Comp., 22 (2000), pp. 951–985.
- [28] D. HANSEL, G. MATO, AND C. MEUNIER, *Synchrony in excitatory neural networks*, Neural Computation, 7 (1995), pp. 307–337.
- [29] W. B. HAYES, *Rigorous Shadowing of Numerical Solutions of Ordinary Differential Equations by Containment*, PhD thesis, University of Toronto, 2001.
- [30] I. A. HISKENS, *Stability of limit cycles in hybrid systems*, in Proceedings 34th Hawaii International Conference on System Sciences, January 2001.
- [31] A. L. HODGKIN AND A. F. HUXLEY, *Currents carried by sodium and potassium ions through the membrane of the giant axon of Loligo*, Journal of Physiology, 117 (1952), pp. 500–544.
- [32] F. C. HOPPENSTEADT AND E. M. IZHIKEVICH, *Weakly Coupled Neural Networks*, Springer, 1997.
- [33] I. T. JOLLIFFE, *Principal Component Analysis*, Springer, 1986.
- [34] C. JONES, *Geometric singular perturbation theory*, in Dynamical systems, Montecatini Terme, L. Arnold, ed., vol. 1609 of Lecture notes in mathematics, Springer-Verlag, Berlin, 1994, pp. 44–118.
- [35] S. R. JONES, D. J. PINTO, T. J. KAPER, AND N. KOPELL, *Alpha-frequency rhythms desynchronize over long cortical distances: A modeling study*, J. Comp. Neurosci., 9 (2000), pp. 271–291.
- [36] J. P. KEENER, F. C. HOPPENSTEADT, AND J. RINZEL, *Integrate-and-fire models of nerve membrane response to oscillatory input*, SIAM J. Appl. Math., 41 (1981), pp. 503–517.
- [37] J. P. KEENER AND J. SNEYD, *Mathematical Physiology*, Springer, 1998.
- [38] T. B. KEPLER, L. F. ABBOTT, AND E. MARDER, *Reduction of conductance-based neuron models*, Biological Cybernetics, 66 (1992), pp. 381–387.
- [39] W. M. KISTLER, W. GERSTNER, AND J. L. VAN HEMMEN, *Reduction of the Hodgkin-Huxley equations to a single-variable threshold model*, Neural Computation, 9 (1997), pp. 1015–1045.
- [40] C. KOCH, O. BERNANDER, AND R. J. DOUGLAS, *Do neurons have a voltage or a current threshold for action potential initiation?*, Journal of Computational Neuroscience, 2 (1995), pp. 63–82.
- [41] N. KOPELL AND G. B. ERMENTROUT, *Symmetry and phaselocking in chains of weakly coupled oscillators*, Commun. Pure Appl. Math., 39 (1986), pp. 623–660.
- [42] ———, *Coupled oscillators and the design of central pattern generators*, Math. Biosci., 90 (1988), pp. 87–109.
- [43] N. KOPELL AND G. LEMASSON, *Rhythmogenesis, amplitude modulation and multiplexing in a cortical architecture*, Proc. Natl. Acad. Sci. USA, 88 (1994), pp. 897–901.
- [44] M. KRUPA AND P. SZMOLYAN, *Relaxation oscillation and canard explosion*, J. Diff. Eq., 174 (2001).
- [45] Y. KURAMOTO, *Collective synchronization of pulse-coupled oscillators and excitable units*, Physica D, 50 (1991), pp. 15–30.
- [46] L. LAPIQUE, *Recherches quantitatives sur l’excitation électriques des nerfs traitée comme une polarization*, J. Physiol. Pathol. Gen., 9 (1907), pp. 620–635.
- [47] U. MAAS AND S. B. POPE, *Simplifying chemical kinetics: Intrinsic low dimensional manifolds in composition space*, Combustion and Flame, 88 (1992), pp. 239–264.
- [48] H. MCKEAN, *Nagumo’s equation*, Advances in mathematics, 4 (1970), pp. 209–223.
- [49] R. MIROLLO AND S. STROGATZ, *Synchronization of pulse-coupled biological oscillators*, SIAM J. Appl. Math., 50 (1990), pp. 1645–1662.
- [50] E. F. MISHCHENKO AND N. K. ROZOV, *Differential Equations with Small Parameters and Relaxation Oscillators*, Plenum Press, New York, 1980.
- [51] C. MORRIS AND H. LECAR, *Voltage oscillations in the barnacle giant muscle fiber*, Biophysical Journal, 35 (1981), pp. 193–213.
- [52] J. D. MURRAY, *Mathematical Biology*, Springer-Verlag, Heidelberg, 1989.
- [53] S. Y. PILYUGIN, *Shadowing in Dynamical Systems*, vol. 1706 of Lect. Notes in Math., Springer, 1999.
- [54] M. RATHINAM AND L. R. PETZOLD, *Dynamic iteration using reduced order models: A method for simulation of large scale modular systems*, SIAM J. Numer. Anal., 40 (2002), pp. 1446–1474.
- [55] ———, *A new look at proper orthogonal decomposition*, SIAM J. Numer. Anal., 41 (2003), pp. 1893–1925.
- [56] M. J. REWIEŃSKI, *A Trajectory Piecewise-Linear Approach to Model Order Reduction of Nonlinear Dynamical Systems*, PhD thesis, Technical University of Gdańsk, Poland, 1998.
- [57] H. G. ROTSTEIN, R. CLEWLEY, M. WECHSELBERGER, AND N. KOPELL, *Dynamics of an entorhinal cortex stellate cell model*. In preparation.
- [58] H. G. ROTSTEIN, M. J. GILLIES, C. D. ACKER, J. A. WHITE, M. A. WHITTINGTON, AND N. KOPELL, *Slow and fast inhibition and H-current interact to create a theta rhythm in a model of CA1 interneuron networks*. Submitted.
- [59] C. W. ROWLEY, *Model reduction for fluids, using balanced proper orthogonal decomposition*, Int. J. on Bifurcation and Chaos, (2005). To appear.
- [60] R. SUCKLEY AND V. BIKTASHEV, *The asymptotic structure of the Hodgkin-Huxley equations*, Int. J. Bifurcation & Chaos, 13 (2003), pp. 3805–3826.

- [61] ———, *Comparison of asymptotics of heart and nerve excitability*, Phys. Rev. E, (2003).
- [62] D. C. TARRAF AND H. H. ASADA, *On the nature and stability of differential-algebraic systems*, in Proc. of American Control Conf., May 2002.
- [63] J. H. TAYLOR AND D. KEBEDE, *Modeling and simulation of hybrid systems in Matlab*, in Proc. IFAC World Congress, July 1996.
- [64] B. VAN DER POL, *Forced oscillations in a circuit with nonlinear resistance (receptance with reactive triode)*, in Selected Papers on Mathematical Trends in Control Theory, R. Bellman and R. Kalaba, eds., Dover, 1964. Reprint of article in the London, Edinburgh and Dublin Phil. Mag., 3(65–80), 1927.
- [65] A. VAN DER SCHAFT AND H. SCHUMACHER, *An Introduction to Hybrid Dynamical Systems*, Springer-Verlag, 1999.
- [66] X.-J. WANG AND G. BUZSÁKI, *Gamma oscillation by synaptic inhibition in a hippocampal interneuronal network model*, Journal of Neuroscience, 16 (1996), pp. 6402–6413.
- [67] J. WHITE, C. CHOW, J. RITT, C. SOTO-TREVIÑO, AND N. KOPELL, *Synchronization and oscillatory dynamics in heterogeneous, mutually inhibited neurons*, J. Comp. Neurosci., 5 (1998), pp. 5–16.
- [68] M. WHITTINGTON, R. D. TRAUB, AND J. JEFFERYS, *Synchronized oscillations in interneuron networks driven by metabotropic glutamate receptor activation*, Nature, 373 (1995), pp. 612–615.
- [69] M. WHITTINGTON, R. D. TRAUB, N. KOPELL, B. ERMENTROUT, AND E. BUHL, *Inhibition-based rhythms: experimental and mathematical observations on network dynamics*, International Journal of Psychophysiology, 38 (2000), pp. 315–336.
- [70] S. WIGGINS, *Normally Hyperbolic Invariant Manifolds in Dynamical Systems*, Springer-Verlag, New York, 1994.
- [71] H. R. WILSON AND J. D. COWAN, *A mathematical theory of the functional dynamics of cortical and thalamic nervous tissue*, Kybernetik, 13 (1973), pp. 55–80.
- [72] A. WINFREE, ed., *The Geometry of Biological Time*, Springer-Verlag, New York, 1980.